Enhanced Spin Coherence of a Self-Assembled Quantum Dot Molecule at the Optimal Electrical Bias

Kha X. Tran, Allan S. Bracker, Michael K. Yakes, Joel Q. Grim, and Samuel G. Carter

Phys. Rev. Lett. **129**, 027403 — Published 7 July 2022

DOI: 10.1103/PhysRevLett.129.027403

Enhanced spin coherence of a self-assembled quantum dot molecule at the optimal electrical bias

Kha X. Tran,[1] Allan S. Bracker,[2] Michael K. Yakes,[2†] Joel Q. Grim,[2], and Samuel G. Carter[2,*]
[1] NRC Research Associate at the Naval Research Laboratory, 4555 Overlook Ave. SW, Washington, DC 20375, USA
[2] Naval Research Laboratory, 4555 Overlook Ave. SW, Washington, DC 20375, USA

[†]Present address: Air Force Office of Scientific Research, Arlington, VA 22203, USA.
*sam.carter@nrl.navy.mil

Abstract:

A pair of coupled dots with one electron in each dot can provide improvements in spin coherence, particularly at an electrical bias called the "sweet spot", but few measurements have been performed on self-assembled dots in this regime. Here, we directly measure the T_2^* coherence time of the singlet-triplet states in this system as a function of bias and magnetic field, obtaining a maximum T_2^* of 60 ns, more than an order of magnitude higher than an electron spin in a single quantum dot. Our results uncover two main dephasing mechanisms: electrical noise away from the sweet spot, and a magnetic field dependent interaction with nuclear spins due to a difference in g-factors.

Main text:

The electron spin in an InGaAs self-assembled quantum dot (QD) is a promising candidate for quantum applications due to bright, spin-dependent optical transitions, fast optical control, integration, and potential scalability [1]. QDs are readily grown by molecular beam epitaxy and can be integrated into nanophotonic structures containing both electronic [2] and photonic circuit elements [3,4]. However, the electron spin in a QD is prone to decoherence, primarily due to interactions with the nuclear spin bath [5–7]. Without advanced spectroscopy techniques [8–14] to limit the effect of these interactions, the coherence time of a QD single spin is very short, i.e. a few nanoseconds [8,15,16], which severely limits its use.

One way to extend the coherence time in the semiconductor QD is to utilize the two electron spins in the coupled quantum dot system, which consists of the top and bottom dot separated by a tunneling barrier. The electrons hybridize and form the bonding and anti-bonding states, hence the name quantum dot molecule (QDM) [17–22]. The two electrons interact strongly with each other via the electron-electron exchange, which splits the energy degeneracy between the singlet (S) and triplet (T_0, T+, T-) ground states. The $m_s = 0$ S and T_0 states are in principle insensitive to fluctuating magnetic fields from nuclear spins [23], but the exchange splitting does depend on the electric field, making it sensitive to electric field fluctuations [24]. As a function of electrical bias, the QDM features a sweet spot which is the location of minimum exchange interaction where the S-T_0 subspace is first order immune to both electric and magnetic field fluctuations [23,25,26]. Indeed, operating at the sweet spot has proved to be a viable strategy to extend the coherence time of the electron spin. In one optically active QDM, T_2^* was shown to have an upper limit of about 200 ns which was measured in the frequency domain using the coherent population trapping (CPT) technique [23]. Extracting T_2^* from the CPT measurement, however, involves modelling a complicated eight-level system with a number of fitting parameters. This procedure has given a wide range of T_2^* being reported [23].

In this letter, we measure T_2^* directly at the sweet spot using Ramsey interferometry, a time domain technique. Extracting T_2^* only involves a simple curve fit to the data leading to much improved uncertainty and more reliable results. We demonstrate a T_2^* coherence time of 60 ns, the longest value for an optically active QD that has been measured directly. We uncover two main dephasing mechanisms by examining T_2^* as a function of electrical bias as well as the external magnetic field. The dephasing rate from electric field fluctuations is proportional to the derivative of the exchange interaction with respect to the electrical bias. This suggests that the slow electrical noise gives rise to fluctuations in the exchange splitting and limits the coherence away from the sweet spot [24]. Near the sweet spot, the coherence time is limited by the hyperfine interaction with nuclear spins, which has a strong effect at very low magnetic fields, due to mixing of triplet states, and also a strong effect at high magnetic fields, due to an effective magnetic field gradient [27] stemming from the g-factor difference between the two dots. This gives rise to a maximum T_2^* at a modest magnetic field of 50 mT. To the best of our knowledge, this is the first report that measures T_2^* directly, and shows a huge enhancement at the sweet spot in the InGaAs QDM.

Our device, which is schematically depicted in Fig. S1, is grown epitaxially and is embedded in a Bragg cavity with the n-i-p-i-p diode structure that allows the QDM to be deterministically charged with two electrons [28,29]. The sample is positioned at the center of a superconducting magnet ∼3 K which exerts an external magnetic field in the Faraday geometry. With one electron residing in each dot, the spin singlet (S) and spin triplet (T_0, T+, T-) ground states together with the trion excited states (R±, R± ±) form an eight-level system as shown in Fig. 1(a). To achieve electron tunneling, our QDM sample is designed so that the bottom dot transition energy is blue-shifted compared to that of the top dot [18,29]. Thus, we denote the blue (red) arrow as the bottom (top) dot spin [Fig. 1(a)]. The single (double) arrow refers to electron (hole). Due to the optical selection rules, there are six allowed transitions with two pairs of them 1,1* and 3,3* being nearly degenerate. The energy splitting between 1 and 1*(3 and 3*) can only be resolved under high magnetic field [Fig. S7]. We label and color code the transitions from 1 to 4 in the order of increasing energy.

Fig. 1(b) depicts the bias map of the resonance fluorescence (RF) spectra taken at 1 T magnetic field showing the corresponding transitions 1 to 4. The two electron charge state is found to be stable for a bias range of 0.7 to 0.76 V. The RF signal is suppressed in the middle of the stable bias range due to optical spin pumping [30–33] where the spin is excited out of one spin state and shelved in the other after a few recombination cycles. The transition 1* and 3* are still relatively bright in the optical pumping region due to the fact that T-↔R-- and T+↔R++ are cycling transitions [34]. The exchange interaction i.e. the energy splitting between S and T_0 states, denoted by J can be measured directly by taking the energy difference between transition 2 and 1 or transition 4 and 3. The change in relative energy levels of the electron residing in each dot with respect to the electric field leads to a J that is dependent on the gate voltage. In this sample, we find the minimum J (~ 45 μeV) (the sweet spot) to be at the center of the optical pumping region (0.725 V).

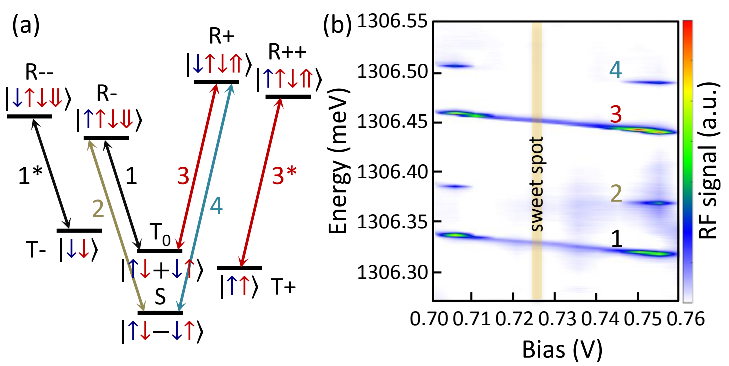

FIG. 1 (color online). (a) Detailed energy-level diagram of the two-electron charged QDM in the Faraday external magnetic field with numbering scheme depicting individual transitions. The spin configuration for each state is also indicated. Here, blue (red) arrow refers to the bottom (top) dot. Single (double) arrow refers to electron (hole). (b) Measured resonance fluorescence spectra as functions of bias. The transitions are identified with numbering and colors that match part (a). The sweet spot is at the center of the optical pumping region (about 0.725 V bias).

To perform electron spin control, we utilize the Λ system T_0↔R-↔S as shown in Fig. 2(a). The linearly polarized initialization laser (70 ns duration) resonant with T_0↔R- and T-↔R-- transitions pumps the spin into the S state [35]. Then, a circularly polarized rotation laser detuned from the excited state (Δ_L~250 GHz) coherently rotates the spin between S and T_0 states, depending on the pulse duration and peak power. Finally, the T_0 population is detected by monitoring the emission from the Raman transition S↔R-. Please see the Supplemental Material for detailed signal filtering and data acquisition [29]. We modulate the rotation laser by a microwave source via an electro-optic modulator (EOM) biased to zero transmission, which creates two side bands in the laser spectrum [12,36]. The side bands energy spacing is twice the modulation frequency, and thus can be varied to detune from the ST_0 exchange splitting a variable amount δ. We note that the energy levels in Fig. 2(a) are not drawn to scale. In reality, Δ_L~250 GHz is about three order of magnitude larger than δ which is only tens to hundreds of MHz. Fig. 2(b) shows the evolution of the T_0 population which is normalized to 1 for increasing rotation pulse duration at four different rotation peak powers. Here, the microwave modulation is slightly detuned from the spin resonance. Thus, the linear fit to the Rabi frequency vs. peak power yields ~28.5 MHz y-intercept [Fig. 2(c)]. Low laser peak power and the relatively large laser detuning Δ_L~250 GHz ensures that we are largely in the adiabatic limit where the excited states population is negligible [12,37].

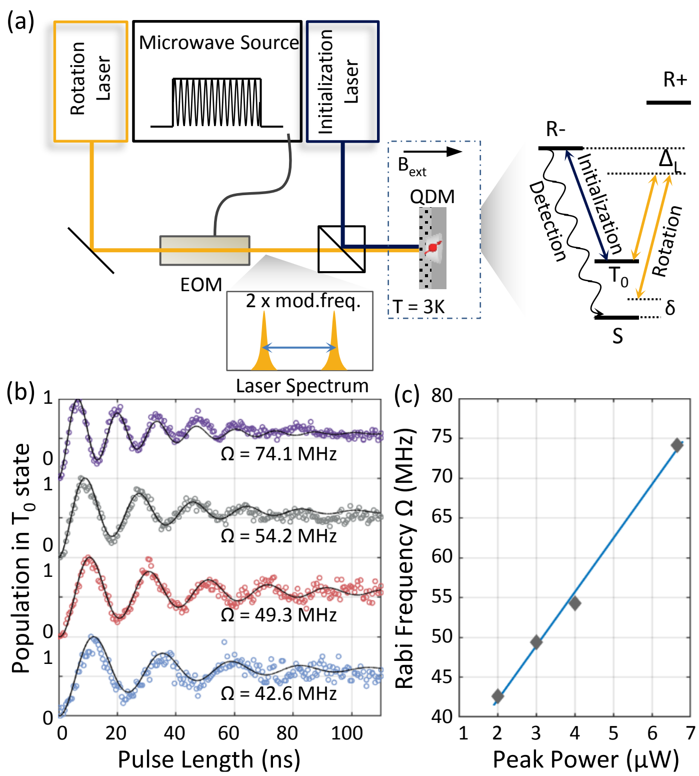

FIG. 2 (color online). (a) Experimental schematic: Intensity modulation of the rotation laser by a microwave source via the electro-optical modulator (EOM) creates two laser side bands whose energy difference is twice the modulation frequency. The rotation laser is detuned $\Delta_L \approx 250$ GHz from the excited state, and the side band energy spacing is detuned δ from the S-T_0 resonance. The initialization laser is resonant with T_0↔R- transition. The T_0 state population is then detected via Raman scattering S↔R-. (b) Rabi oscillations between S and T_0 spin states at four different Rabi frequencies. (c) The dependence of the Rabi frequency on the peak power of the rotation laser.

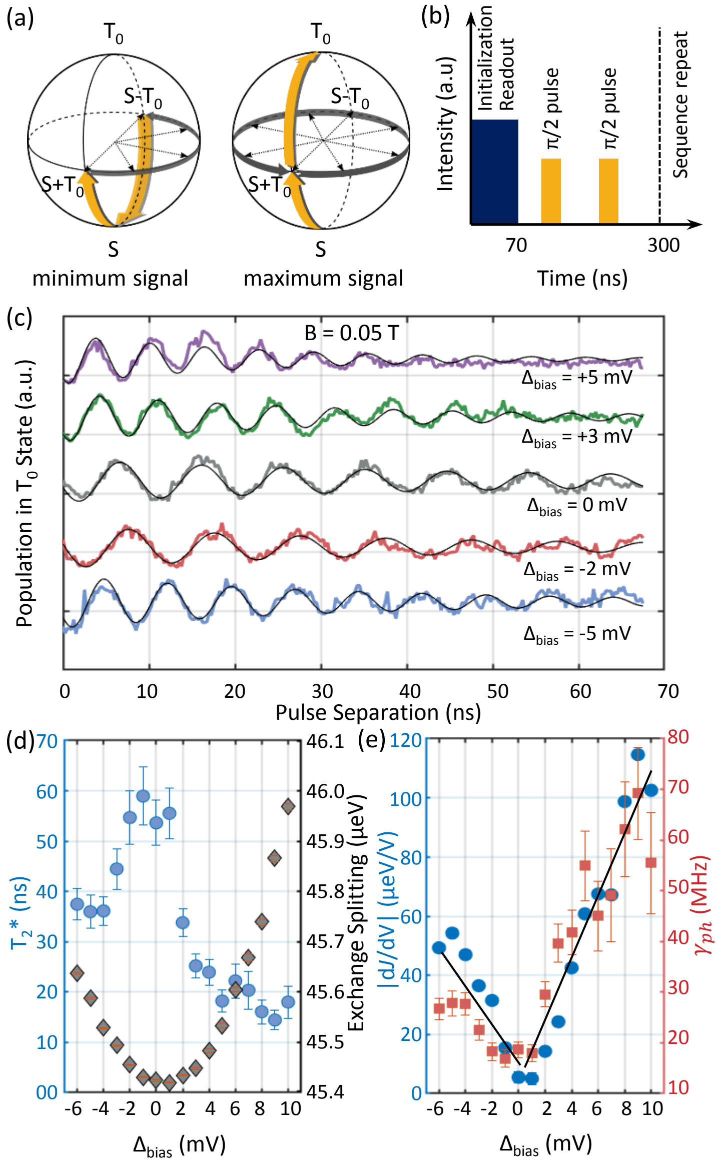

FIG. 3 (color online). (a) Bloch sphere representation of spin control of the ST_0 subspace. (b) The pulse sequence for Ramsey measurement which consists of a 70 ns initialization pulse, and two π/2 rotation pulses (2.5 ns duration) with variable separation between them. The sequence is repeated after every 300 ns. (c) Ramsey interference obtained at B = 0.05 T and at various biases Δ_{bias} relative to the sweet spot. The data is fitted with exponential oscillation decay (black solid lines). (d) T_2^* (left vertical axis) and S-T_0 energy splitting (right vertical axis) are extracted from the Ramsey interference data and are plotted as functions of the bias offset from the sweet spot. (e) The dephasing rate (γ_{ph}) and magnitude of the derivative of the exchange splitting with respect to bias (|dJ/dV|) are plotted against the bias offset from the sweet spot showing a linear correlation between the two quantities.

To measure the coherence time T_2^*, we employ the Ramsey interferometry technique which is schematically shown in Fig. 3(a-b). The spin is initialized to the S state (south pole). The first π/2 rotation pulse (2.5 ns) creates the coherent superposition of S and T_0 states which then precesses and decays in a characteristic time scale T_2^*. A second π/2 rotation pulse converts the coherence into a population difference, which is read out by the initialization/readout pulse. As the separation between the two rotation pulses increases, the phase difference between the superposition and the second π/2 pulse increases, leading to a final state oscillating between T_0 (maximum signal) and S(minimum signal). Fig. 3(c) shows the Ramsey interference curves for five different bias offsets Δ_{bias} from the sweet spot at a relatively low magnetic field 0.05 T. In these measurements, we deliberately red-detune the microwave modulation frequency away from the ST_0 energy splitting by a few hundred megahertz. The detuning δ gives rise to oscillations in the Ramsey signal that are fit to precisely determine δ. The exchange splitting J is then computed from δ and the microwave modulation frequency ω_m by the formula: $J = 2\omega_m + \delta$. Although in principle J can be measured directly from the RF data in Fig. 1(b), optical pumping makes it difficult to determine J around the sweet spot. Using the Ramsey interference oscillations, we can extract J and T_2^* precisely [Fig. 3(d)] with T_2^* given by the exponential decay of the fringe contrast.

We see a dramatic enhancement of T_2^* in the vicinity of the sweet spot [Fig. 3(d)] with the maximum value of almost 60 ns. This value is comparable to that of the electrostatically confined GaAs QDM [9,24] taken at much lower temperature. An important question remains: what factors limit the coherence in our sample? As the spin relaxation time T_1 exceeds 1.5 μs in the optical pumping bias range, T_1 decay is not an important source of decoherence [29]. As mentioned previously, dephasing will occur from fluctuations in the bias voltage ΔV_{noise} (from the source or the local environment) that lead to fluctuations in J [26,38,39]. To first order in the bias fluctuations, the dephasing rate is given by $\gamma_{\text{elec}} = (dJ/dV)\,\Delta V_{noise}$. Indeed, we see a strong linear correlation between the dephasing rate denoted $\gamma_{ph} = 1/T_2^*$ and the derivative of J with respect to the bias voltage V as shown in Fig. 3(e). From fitting this data, we extract $\Delta V_{noise} = 1.836 \pm 0.0262$ mV, which signifies the voltage fluctuation in our QDM. A bias-independent offset is included in the fit, with a value of 14.83 ± 3.732 MHz, to account for other sources of dephasing. This linear correlation strongly suggests that voltage noise is the primary dephasing mechanism away from the sweet spot [24,40]. This noise is expected to have a low frequency spectrum compared to the dephasing rate. We also attempt to partially bypass this noise source by apply a spin-echo pulse sequence and indeed measure much longer T_2, up to 500 ns as shown in the Supplemental Material [29,41,42].

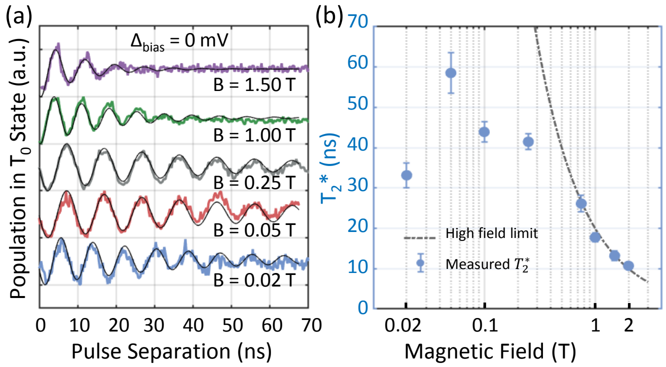

FIG. 4 (color online). (a) Ramsey interference data obtained at the sweet spot at various magnetic field strength. (b) Semilog plot of T_2^* against the magnetic field. Dotted curve denotes the expected change of T_2^* at high field regime.

We suspect that the dephasing rate at the sweet spot is due to fluctuations in the nuclear spin environment. To investigate this possibility, we measure T_2^* for a series of magnetic fields and plot the results at the sweet spot in Fig 4. The coherence time peaks at 0.05 T and decreases precipitously once the field deviates from it. At the low field regime, the nuclear polarization can exceed the Zeeman splitting between triplets (T_0, T+, T-) and thus, strongly mix them leading to rapid dephasing [23]. On the other hand, high fields cause mixing between S and T_0 due to an effective field gradient stemming from the difference in g-factor between two dots. It leads to the dependence of the exchange splitting on B which has been explored theoretically [27] and experimentally [43]. In fact, if the gradient field is much stronger than the exchange interaction, the eigenstates would become the product states $|\uparrow\downarrow\rangle$ and $|\downarrow\uparrow\rangle$ of the two independent spins, in which we would exactly recover the dephasing of the single spin. The exchange splitting of the new eigenstates is modified by: $J' = \sqrt{J^2 + 4(\Delta g \mu_B B)^2}$. Here, J is the exchange splitting at zero field; μ_B is the Bohr magneton; Δg is the g-factor difference which can be measured directly by looking at the energy difference between T_0↔R+ and T+↔R++ or T_0↔R- and T-↔R-- at high magnetic field. In Fig. S7, we measure PL at 6 T and extract the average $\Delta g \mu_B$ of 0.3 GHz/T which is about 5% of the electron spin g-factor in an isolated dot [44].

Similar to the case of bias fluctuations, we expect the dephasing rate from nuclear spin fluctuations in the high field regime to be given by $\gamma_{\text{nuc}} = \frac{dJ'}{d(\Delta g \mu_B B)} \Delta E_{nuc} \cong \frac{4\Delta g \mu_B B}{J} \Delta E_{nuc}$, where ΔE_{nuc} is the fluctuation in the difference in nuclear field energies between the two dots. The typical Overhauser field in QD is 20 mT [5–7] which gives ΔE_{nuc} of 120 MHz. We thus expect γ_{nuc}/B=13 MHz/T which is an order of magnitude in agreement with the measured dephasing rate at high fields i.e. $\gamma_{ph}/B \cong 50$ MHz/T at 2 T. This rough estimate of the expected dephasing contribution is plotted in Fig. 4(b), which matches quite well with the trend of the rapid dephasing at high fields after multiplying by a scaling factor. At moderate fields, the measured T_2^* is much shorter than expected from this contribution, due to low field mixing of triplet states. The maximum T_2^* occurs in an intermediate regime that balances dephasing from triplet mixing and dephasing from singlet-triplet mixing, due to Δg.

In summary, we present a systematic study of the coherence time T_2^* in self-assembled QDM and demonstrate more than an order of magnitude improvement over electron spins in single QDs. We find that the electrical fluctuations mainly limit the spin coherence at biases away from the sweet spot. At the sweet spot, the nuclear spin fluctuations are largely responsible for dephasing in both low and high magnetic field regimes. Decreasing the impact of the nuclear spin fluctuations requires operating at magnetic fields larger than the nuclear fields that mix triplet states but not so large that differences in the g-factors give rise to singlet-triplet mixing. This singlet-triplet mixing can be avoided by reducing Δg, perhaps through growth of QDs with more similar thicknesses, and by increasing J. By reducing the tunnel barrier thickness or height, J can be increased to several meV, but this must be balanced against the decreased spin relaxation times typically observed in these structures [23,40,45,46]. Improved spin coherence times for self-assembled QDs should enable a variety of applications in quantum photonics that require a quantum memory, such as photonic cluster state generation [47,48] and single photon switches and transistors [49].

Acknowledgements: We gratefully acknowledge helpful discussions with Edo Waks and Dima Farfurnik. This work was supported by the U.S. Office of Naval Research, the Defense Threat Reduction Agency (Grant No. HDTRA1-15-1-0011).

References

[1] R. J. Warburton, *Single Spins in Self-Assembled Quantum Dots*, Nat. Mater. **12**, 483 (2013).

[2] R. J. Warburton, C. Schäflein, D. Haft, F. Bickel, A. Lorke, K. Karrai, J. M. Garcia, W. Schoenfeld, and P. M. Petroff, *Optical Emission from a Charge-Tunable Quantum Ring*, Nature **405**, 926 (2000).

[3] D. Englund, A. Faraon, B. Zhang, Y. Yamamoto, and J. Vuckovic, *Generation and Transfer of Single Photons on a Photonic Crystal Chip*, Opt. Express **15**, 5550 (2007).

[4] J. Q. Grim et al., *Scalable in Operando Strain Tuning in Nanophotonic Waveguides Enabling Three-Quantum-Dot Superradiance*, Nat. Mater. **18**, 963 (2019).

[5] A. V. Khaetskii, D. Loss, and L. Glazman, *Electron Spin Decoherence in Quantum Dots Due to Interaction with Nuclei*, Phys. Rev. Lett. **88**, 186802 (2002).

[6] I. A. Merkulov, Al. L. Efros, and M. Rosen, *Electron Spin Relaxation by Nuclei in Semiconductor Quantum Dots*, Phys. Rev. B **65**, 205309 (2002).

[7] B. Urbaszek, X. Marie, T. Amand, O. Krebs, P. Voisin, P. Maletinsky, A. Högele, and A. Imamoglu, *Nuclear Spin Physics in Quantum Dots: An Optical Investigation*, Rev. Mod. Phys. **85**, 79 (2013).

[8] D. Press, K. De Greve, P. L. McMahon, T. D. Ladd, B. Friess, C. Schneider, M. Kamp, S. Höfling, A. Forchel, and Y. Yamamoto, *Ultrafast Optical Spin Echo in a Single Quantum Dot*, Nat. Photonics **4**, 367 (2010).

[9] J. R. Petta, A. C. Johnson, J. M. Taylor, E. A. Laird, A. Yacoby, M. D. Lukin, C. M. Marcus, M. P. Hanson, and A. C. Gossard, *Coherent Manipulation of Coupled Electron Spins in Semiconductor Quantum Dots*, Science **309**, 2180 (2005).

[10] X. Xu, W. Yao, B. Sun, D. G. Steel, A. S. Bracker, D. Gammon, and L. J. Sham, *Optically Controlled Locking of the Nuclear Field via Coherent Dark-State Spectroscopy*, Nature **459**, 1105 (2009).

[11] C. Latta et al., *Confluence of Resonant Laser Excitation and Bidirectional Quantum-Dot Nuclear-Spin Polarization*, Nat. Phys. **5**, 758 (2009).

[12] J. H. Bodey, R. Stockill, E. V. Denning, D. A. Gangloff, G. Éthier-Majcher, D. M. Jackson, E. Clarke, M. Hugues, C. L. Gall, and M. Atatüre, *Optical Spin Locking of a Solid-State Qubit*, Npj Quantum Inf. **5**, 95 (2019).

[13] D. A. Gangloff, G. Éthier-Majcher, C. Lang, E. V. Denning, J. H. Bodey, D. M. Jackson, E. Clarke, M. Hugues, C. L. Gall, and M. Atatüre, *Quantum Interface of an Electron and a Nuclear Ensemble*, Science **364**, 62 (2019).

[14] F. H. L. Koppens, K. C. Nowack, and L. M. K. Vandersypen, *Spin Echo of a Single Electron Spin in a Quantum Dot*, Phys. Rev. Lett. **100**, 236802 (2008).

[15] X. Xu, B. Sun, P. R. Berman, D. G. Steel, A. S. Bracker, D. Gammon, and L. J. Sham, *Coherent Population Trapping of an Electron Spin in a Single Negatively Charged Quantum Dot*, Nat. Phys. **4**, 692 (2008).

[16] A. Greilich, D. R. Yakovlev, A. Shabaev, Al. L. Efros, I. A. Yugova, R. Oulton, V. Stavarache, D. Reuter, A. Wieck, and M. Bayer, *Mode Locking of Electron Spin Coherences in Singly Charged Quantum Dots*, Science **313**, 341 (2006).

[17] M. Scheibner, A. S. Bracker, D. Kim, and D. Gammon, *Essential Concepts in the Optical Properties of Quantum Dot Molecules*, Solid State Commun. **149**, 1427 (2009).

[18] E. A. Stinaff, M. Scheibner, A. S. Bracker, I. V. Ponomarev, V. L. Korenev, M. E. Ware, M. F. Doty, T. L. Reinecke, and D. Gammon, *Optical Signatures of Coupled Quantum Dots*, Science **311**, 636 (2006).

[19] M. F. Doty, M. Scheibner, A. S. Bracker, I. V. Ponomarev, T. L. Reinecke, and D. Gammon, *Optical Spectra of Doubly Charged Quantum Dot Molecules in Electric and Magnetic Fields*, Phys. Rev. B **78**, 115316 (2008).

[20] P. Kumar, C. Jennings, M. Scheibner, A. S. Bracker, S. G. Carter, and D. Gammon, *Spectral Broadening of Optical Transitions at Tunneling Resonances in InAs/GaAs Coupled Quantum Dot Pairs*, Phys. Rev. B **102**, 085423 (2020).

[21] H. J. Krenner, E. C. Clark, T. Nakaoka, M. Bichler, C. Scheurer, G. Abstreiter, and J. J. Finley, *Optically Probing Spin and Charge Interactions in a Tunable Artificial Molecule*, Phys. Rev. Lett. **97**, 076403 (2006).

[22] E. Zallo, R. Trotta, V. Křápek, Y. H. Huo, P. Atkinson, F. Ding, T. Šikola, A. Rastelli, and O. G. Schmidt, *Strain-Induced Active Tuning of the Coherent Tunneling in Quantum Dot Molecules*, Phys. Rev. B **89**, 241303 (2014).

[23] K. M. Weiss, J. M. Elzerman, Y. L. Delley, J. Miguel-Sanchez, and A. Imamoğlu, *Coherent Two-Electron Spin Qubits in an Optically Active Pair of Coupled InGaAs Quantum Dots*, Phys. Rev. Lett. **109**, 107401 (2012).

[24] O. E. Dial, M. D. Shulman, S. P. Harvey, H. Bluhm, V. Umansky, and A. Yacoby, *Charge Noise Spectroscopy Using Coherent Exchange Oscillations in a Singlet-Triplet Qubit*, Phys. Rev. Lett. **110**, 146804 (2013).

[25] M. Stopa and C. M. Marcus, *Magnetic Field Control of Exchange and Noise Immunity in Double Quantum Dots*, Nano Lett. **8**, 1778 (2008).

[26] X. Hu and S. Das Sarma, *Charge-Fluctuation-Induced Dephasing of Exchange-Coupled Spin Qubits*, Phys. Rev. Lett. **96**, 100501 (2006).

[27] J.-T. Hung, Ł. Cywiński, X. Hu, and S. Das Sarma, *Hyperfine Interaction Induced Dephasing of Coupled Spin Qubits in Semiconductor Double Quantum Dots*, Phys. Rev. B **88**, 085314 (2013).

[28] A. S. Bracker, M. Scheibner, M. F. Doty, E. A. Stinaff, I. V. Ponomarev, J. C. Kim, L. J. Whitman, T. L. Reinecke, and D. Gammon, *Engineering Electron and Hole Tunneling with Asymmetric InAs Quantum Dot Molecules*, Appl. Phys. Lett. **89**, 233110 (2006).

[29] See Supplemental Material for details of the sample fabrication, and methods.

[30] X. Xu, Y. Wu, B. Sun, Q. Huang, J. Cheng, D. G. Steel, A. S. Bracker, D. Gammon, C. Emary, and L. J. Sham, *Fast Spin State Initialization in a Singly Charged InAs-GaAs Quantum Dot by Optical Cooling*, Phys. Rev. Lett. **99**, 097401 (2007).

[31] D. Kim, S. E. Economou, Ş. C. Bădescu, M. Scheibner, A. S. Bracker, M. Bashkansky, T. L. Reinecke, and D. Gammon, *Optical Spin Initialization and Nondestructive Measurement in a Quantum Dot Molecule*, Phys. Rev. Lett. **101**, 236804 (2008).

[32] M. Atatüre, J. Dreiser, A. Badolato, A. Högele, K. Karrai, and A. Imamoglu, *Quantum-Dot Spin-State Preparation with Near-Unity Fidelity*, Science **312**, 551 (2006).

[33] S. G. Carter, S. C. Badescu, A. S. Bracker, M. K. Yakes, K. X. Tran, J. Q. Grim, and D. Gammon, *Coherent Population Trapping Combined with Cycling Transitions for Quantum Dot Hole Spins Using Triplet Trion States*, Phys. Rev. Lett. **126**, 107401 (2021).

[34] Y. L. Delley, M. Kroner, S. Faelt, W. Wegscheider, and A. İmamoğlu, *Spin Measurement Using Cycling Transitions of a Two-Electron Quantum Dot Molecule*, ArXiv150904171 Cond-Mat (2015).

[35] To completely initialize the system into S state, one would need another initialization laser resonant to T_0↔R+ and T+↔R++. But for the purpose of our experiment, one initialization laser is suffice.

[36] Y.-M. He et al., *Coherently Driving a Single Quantum Two-Level System with Dichromatic Laser Pulses*, Nat. Phys. **15**, 941 (2019).

[37] D. Press, T. D. Ladd, B. Zhang, and Y. Yamamoto, *Complete Quantum Control of a Single Quantum Dot Spin Using Ultrafast Optical Pulses*, Nature **456**, 7219 (2008).

[38] A. P. Higginbotham, F. Kuemmeth, M. P. Hanson, A. C. Gossard, and C. M. Marcus, *Coherent Operations and Screening in Multielectron Spin Qubits*, Phys. Rev. Lett. **112**, 026801 (2014).

[39] D. Culcer, X. Hu, and S. Das Sarma, *Dephasing of Si Spin Qubits Due to Charge Noise*, Appl. Phys. Lett. **95**, 073102 (2009).

[40] D. Kim, S. G. Carter, A. Greilich, A. S. Bracker, and D. Gammon, *Ultrafast Optical Control of Entanglement between Two Quantum-Dot Spins*, Nat. Phys. **7**, 223 (2011).

[41] X. Hu, *Two-Spin Dephasing by Electron-Phonon Interaction in Semiconductor Double Quantum Dots*, Phys. Rev. B **83**, 165322 (2011).

[42] K. Roszak and P. Machnikowski, *Phonon-Induced Dephasing of Singlet-Triplet Superpositions in Double Quantum Dots without Spin-Orbit Coupling*, Phys. Rev. B **80**, 195315 (2009).

[43] F. H. L. Koppens, J. A. Folk, J. M. Elzerman, R. Hanson, L. H. W. van Beveren, I. T. Vink, H. P. Tranitz, W. Wegscheider, L. P. Kouwenhoven, and L. M. K. Vandersypen, *Control and Detection of Singlet-Triplet Mixing in a Random Nuclear Field*, Science **309**, 1346 (2005).

[44] A. Schwan, B.-M. Meiners, A. Greilich, D. R. Yakovlev, M. Bayer, A. D. B. Maia, A. A. Quivy, and A. B. Henriques, *Anisotropy of Electron and Hole G-Factors in (In,Ga)As Quantum Dots*, Appl. Phys. Lett. **99**, 221914 (2011).

[45] P. M. Vora, A. S. Bracker, S. G. Carter, T. M. Sweeney, M. Kim, C. S. Kim, L. Yang, P. G. Brereton, S. E. Economou, and D. Gammon, *Spin–Cavity Interactions between a Quantum Dot Molecule and a Photonic Crystal Cavity*, Nat. Commun. **6**, 1 (2015).

[46] J. M. Elzerman, K. M. Weiss, J. Miguel-Sanchez, and A. Imamoğlu, *Optical Amplification Using Raman Transitions between Spin-Singlet and Spin-Triplet States of a Pair of Coupled In-GaAs Quantum Dots*, Phys. Rev. Lett. **107**, 017401 (2011).

[47] D. Scerri, R. N. E. Malein, B. D. Gerardot, and E. M. Gauger, *Frequency-Encoded Linear Cluster States with Coherent Raman Photons*, Phys. Rev. A **98**, 022318 (2018).

[48] I. Schwartz, D. Cogan, E. R. Schmidgall, Y. Don, L. Gantz, O. Kenneth, N. H. Lindner, and D. Gershoni, *Deterministic Generation of a Cluster State of Entangled Photons*, Science **354**, 434 (2016).

[49] S. Sun, H. Kim, Z. Luo, G. S. Solomon, and E. Waks, *A Single-Photon Switch and Transistor Enabled by a Solid-State Quantum Memory*, Science **361**, 57 (2018).